NIH Library Document Request

REG-10057206

Relais

PETER J BASSER
BLDG.13/RM.3N-17

ATTN:
PHONE: 435-1949
FAX:
E-MAIL:

SUBMITTED:
PRINTED: 2003-03-18 06:16:41
REQUEST NO.:REG-10057206
SENT VIA: Manual

REG	Regular	Copy	Journal

DELIVERY: E-mail: pb12q@nih.gov
REPLY: Mail:

THIS IS NOT A BILL.

From the NIH Library in Building 10

MATTIELLO J, BASSER PJ, LEBIHAN D
ANALYTICAL EXPRESSIONS FOR THE B-MATRIX IN NMR DIFFUSION IMAGING AND SPECTROSCOPY
J MAGN RESON SER A 108 (2): 131-141 JUN 1994

JOURNAL OF MAGNETIC RESONANCE, Series A **108**, 131–141 (1994)

Analytical Expressions for the *b* Matrix in NMR Diffusion Imaging and Spectroscopy

JAMES MATTIELLO,* PETER J. BASSER,* AND DENIS LEBIHAN†

** Biomedical Engineering and Instrumentation Program, National Center for Research Resources, and † Diagnostic Radiology Department, Warren G. Magnuson Clinical Center, National Institutes of Health, Bethesda, Maryland 20892*

Received December 22, 1992; revised September 2, 1993

General analytical expressions are presented for the *b* matrix used in diffusion NMR imaging and spectroscopy. These expressions are evaluated in the case of a two-dimensional Fourier-transform spin-echo imaging sequence and show the effect of "cross terms" between gradient pulses. The diagonal and off-diagonal components of the *b* matrix are calculated for the anisotropic diffusion tensor. The proposed analysis allows diffusion coefficients and tensors to be determined accurately and with greater efficiency.

INTRODUCTION

The ability to measure molecular diffusion noninvasively and *in vivo* using magnetic resonance imaging (MRI) has generated great interest and is only beginning to be exploited clinically. Its potential applications include imaging of molecular diffusion, functional assessment, tissue characterization, and treatment monitoring (*1*).

Both diffusion NMR spectroscopy (*2–4*) and imaging (*5–8*) of *in vivo* isotropic media require the determination of the scalar *b* factor from the magnetic field gradient-pulse sequence. The diffusion coefficient, D, can be estimated using the relation

$$\ln\left(\frac{S(b)}{S(0)}\right) = -bD. \qquad [1]$$

Above, $S(0)$ is the echo intensity with no diffusion gradient applied, and $S(b)$ is the echo intensity for a particular diffusion gradient strength.

The *b* factor can easily be calculated analytically for simple pulse sequences used in spectroscopy. However, for complicated imaging pulse sequences that may contain localization, crusher, and diffusion gradients, *b* factors have been evaluated either numerically or experimentally (by calibrating the diffusion coefficient from a phantom material) (*9*). Accurate determination of the *b* factor, taking into account all gradient pulses, is necessary for diffusion measurements.

One complication is that imaging and diffusion gradients interact with one another, producing additional "cross terms" in the *b* factor that, if unaccounted for, can lead to an incorrect estimate of the diffusion coefficient (*10*). Another complication is that, in order to describe effective diffusion in some anisotropic media, such as skeletal muscle (*11*) and brain white matter (*12*), one must use a more general expression than Eq. [1],

$$\ln\left(\frac{S(\mathbf{b})}{S(0)}\right) = -\sum_{i=1}^{3}\sum_{j=1}^{3} b_{ij}D_{ij}, \qquad [2]$$

in which b_{ij} is a component of the *b* matrix, $\mathbf{b}$, and D_{ij} is a component of the effective self-diffusion tensor, $\mathbf{D}$ (*13*). In Eq. [2], one must determine the nine elements of the *b* matrix, rather than one scalar *b* factor.

In this paper, we present analytical expressions for the *b* matrix used in NMR diffusion spectroscopy and imaging for a generalized two-dimensional Fourier-transform spin-echo pulse sequence. For an imaging sequence, we show the effect of cross terms between gradient pulses. Finally, we predict the form of the diagonal and off-diagonal elements of the *b* matrix.

THEORY

Expression for the b Factors

The solution to the Bloch equations for a 90°–180° spin-echo pulsed-gradient NMR experiment with diffusion gradients (*14*) is well known, as is the modification of Stejskal to describe free diffusion in an anisotropic medium (*15*). We use analytical expressions for the gradient-pulse sequences, $\mathbf{G}(t)$, where

$$\mathbf{G}(t) = [G_x(t), G_y(t), G_z(t)], \qquad [3a]$$

and functions of $\mathbf{G}(t)$,

$$\mathbf{F}(t) = \int_0^t \mathbf{G}(t')dt' \qquad [3b]$$

1064-1858/94 $6.00

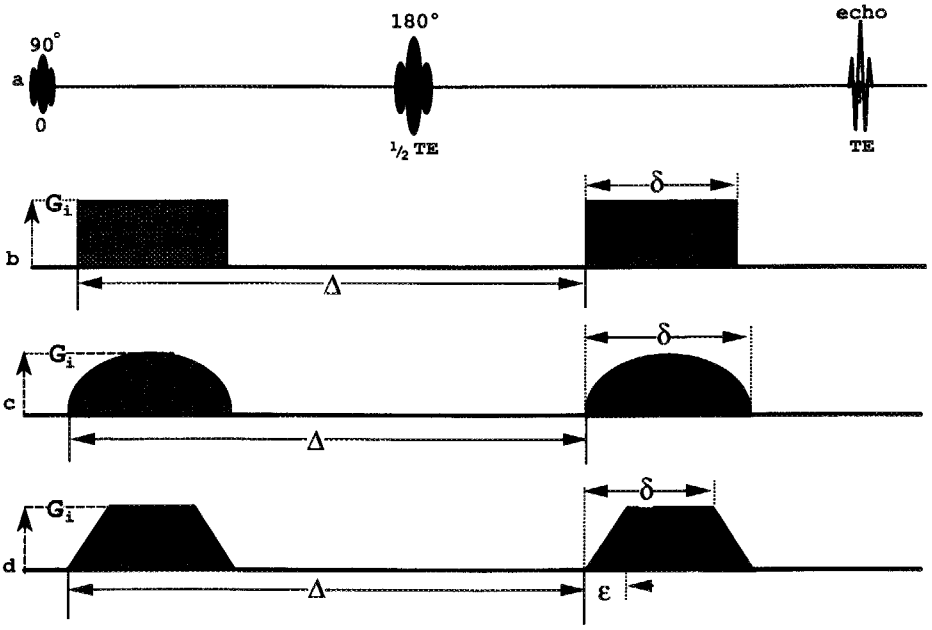

FIG. 1. Spectroscopic gradient-pulse sequences for the 2D FT spin-echo experiment. (a) The 90° and 180° RF pulses and the echo signal are indicated. G_i is the maximum field gradient along the ith coordinate direction. (b) Illustration of rectangular diffusion gradients along one coordinate axis, the x, y, or z direction, where δ is the pulse duration and Δ is the time between the onset of the first and second gradient pulses. (c) Sinusoidal diffusion gradients along one coordinate axis, the x, y, or z direction, where δ is the pulse duration and Δ is the time between the onset of the first and second gradient pulses. (d) Trapezoidal diffusion gradients along one coordinate axis, the x, y, or z direction, where δ is the time between the onset of a trapezoidal pulse and the end of its plateau, ϵ is the rise time of the trapezoidal ramp, and Δ is the time between the onset of the first and second gradient pulses.

and

$$\mathbf{f} = \mathbf{F}(\tfrac{1}{2}\,\mathrm{TE}), \qquad [3c]$$

to derive an analytical expression for the echo intensity, using the formula (*15*)

$$\ln\left(\frac{S}{S(0)}\right) = -\gamma^2 \int_0^{\mathrm{TE}} [\mathbf{F}(t) - 2\xi(t)\mathbf{f}]\mathbf{D}[\mathbf{F}(t) - 2\xi(t)\mathbf{f}]^{\mathrm{T}} dt. \qquad [4]$$

Here, γ is the gyromagnetic ratio, TE is the echo time, $\xi(t) = 0$ when $t < \frac{1}{2}\mathrm{TE}$, $\xi(t) = 1$ when $t \geq \frac{1}{2}\mathrm{TE}$, and $\mathbf{D}$ is the effective or apparent diffusion tensor. The b matrix, $\mathbf{b}$, used in Eq. [2], is given by (*13*)

$$\mathbf{b} = \gamma^2 \int_0^{\mathrm{TE}} [\mathbf{F}(t) - 2\xi(t)\mathbf{f}]^{\mathrm{T}}[\mathbf{F}(t) - 2\xi(t)\mathbf{f}] dt. \qquad [5]$$

Analytical expressions relating the echo intensity and the apparent diffusion tensor are presented for spectroscopic pulse sequences. If G_i and G_j are the maximum field gradients along the ith and jth coordinate directions, respectively, then for a spin-echo sequence in the presence of a constant gradient, the b matrix is

$$b_{ij} = \gamma^2 G_i G_j \mathrm{TE}^3/12. \qquad [6]$$

For a pair of rectangular gradient pulses, with duration δ separated by a time interval Δ, as illustrated in Fig. 1b, the b matrix is

$$b_{ij} = \gamma^2 G_i G_j \delta^2(\Delta - \tfrac{1}{3}\delta). \qquad [7]$$

With a pair of sinusoidal gradient pulses, with duration δ separated by a time interval Δ, as illustrated in Fig. 1c, the b matrix is

$$b_{ij} = \frac{4}{\pi^2}\gamma^2 G_i G_j \delta^2(\Delta - \tfrac{1}{4}\delta). \qquad [8]$$

Finally, for a pair of symmetric trapezoidal pulses like those shown in Fig. 1d, where δ is the time between the initial rise of a trapezoidal pulse and the end of its plateau, Δ is the time between the initial rise of the first and second gradient pulses, and ϵ is the rise time of the trapezoidal ramp, the b matrix is (*13*)

$$b_{ij} = \gamma^2 G_i G_j[\delta^2(\Delta - \tfrac{1}{3}\delta) + \tfrac{1}{30}\epsilon^3 - \tfrac{1}{6}\delta\epsilon^2]. \qquad [9]$$

These formulas reduce to the familiar one-dimensional expressions for isotropic media (*16–19*).

With more complicated imaging pulse sequences, however, Eq. [5] becomes too tedious to evaluate by hand. We therefore used a symbolic manipulation program, similar to that employed by Price and Kuchel (*20*) (who derived simple analytical expressions for scalar b factors in basic diffusion spectroscopy and imaging sequences), to derive analytical expressions for the b matrix for imaging pulse sequences. In evaluating Eq. [5], we have included in the pulse sequence localization, diffusion, and crusher gradients, which are known to affect the echo intensity (*6*).

We synthesize the generalized imaging sequence shown in Fig. 2 from a library of individual sinusoidal and trapezoidal gradient pulses. The parameters, such as gradient pulse shape, intensity, and duration, are described in the note to Table 1. We include all gradient pulses that are typically encountered in 2D FT spin-echo pulse sequences, as shown in Fig. 3.

For a general imaging pulse sequence using trapezoidal diffusion and crusher gradient pulses, as shown in Fig. 2a, the analytical expression for the elements of the b matrix is

$$\begin{aligned} b_{ij} = \gamma^2\{ &\{G_{1i}G_{1j}\}\tau_{11} + \{G_{1i}G_{2j} + G_{2i}G_{1j}\}\tau_{12} \\ &+ \{G_{1i}G_{3j} + G_{3i}G_{1j}\}\tau_{13} + \{G_{1i}G_{4j} + G_{4i}G_{1j}\}\tau_{14} \\ &+ \{G_{1i}G_{5j} + G_{5i}G_{1j}\}\tau_{15} + \{G_{1i}G_{6j} + G_{6i}G_{1j}\}\tau_{16} \\ &+ \{G_{2i}G_{2j}\}\tau_{22} + \{G_{2i}G_{3j} + G_{3i}G_{2j}\}\tau_{23} \\ &+ \{G_{2i}G_{4j} + G_{4i}G_{2j}\}\tau_{24} + \{G_{2i}G_{5j} + G_{5i}G_{2j}\}\tau_{25} \\ &+ \{G_{2i}G_{6j} + G_{6i}G_{2j}\}\tau_{26} + \{G_{3i}G_{3j}\}\tau_{33} \\ &+ \{G_{3i}G_{4j} + G_{4i}G_{3j}\}\tau_{34} + \{G_{3i}G_{5j} + G_{5i}G_{3j}\}\tau_{35} \\ &+ \{G_{3i}G_{6j} + G_{6i}G_{3j}\}\tau_{36} + \{G_{4i}G_{4j}\}\tau_{44} \\ &+ \{G_{4i}G_{5j} + G_{5i}G_{4j}\}\tau_{45} + \{G_{4i}G_{6j} + G_{6i}G_{4j}\}\tau_{46} \\ &+ \{G_{5i}G_{5j}\}\tau_{55} + \{G_{5i}G_{6j} + G_{6i}G_{5j}\}\tau_{56} \\ &+ \{G_{6i}G_{6j}\}\tau_{66}\}. \end{aligned} \quad [10]$$

In this expression for the b matrix, G_{ki} are the gradient intensities. The first index, k, indicates the type of gradient pulse (e.g., slice selection, phase encode, etc.). The second index, i, indicates the coordinate direction in which that pulse is applied (i.e., the read, phase, or slice direction). The τ_{kl}, which are combinations of time intervals and pulse parameters, are defined in Table 1. When the imaging parameters are specified in Eq. [10], one can calculate the elements of the b matrix in each coordinate direction.

We synthesize a generalized imaging pulse sequence using sinusoidal-shaped diffusion and crusher gradient pulses, as shown in Fig. 2b. In this case, the analytical expression for the elements of the b matrix is the same as that in Eq. [10]. The τ_{kl}, which are combinations of the time intervals and pulse parameters, are defined in Table 2.

The plane of the image to be acquired specifies the read, phase, and slice directions with respect to the x-, y-, and z-coordinate directions. For the three basic imaging planes, the following relationships between the axis and image coordinate directions are defined: axial image, x = read, y = phase, and z = slice; sagittal image, x = slice, y = read, and z = phase; and coronal image, x = phase, y = slice, and z = read. For $i = j$, the gradient pulses lie in the same coordinate direction (e.g., in the read direction), while for $i \neq j$, the gradient pulses lie along different coordinate directions (e.g., the read and phase directions). Some of the gradient pulses may be set to zero (i.e., they are not used in a particular coordinate direction). For example, there is no slice-selection gradient in the readout direction. In some cases it is useful to calculate the diagonal and off-diagonal elements of the b matrix separately; Eq. [10] allows for the accurate and quick determination of these elements.

Diagonal Elements of the b Matrix (b_{ii}, $i = j$)

For diffusion in an isotropic medium, in principle, we need only consider the diagonal elements of the b matrix. In this case, a linear relationship exists between the logarithm of the echo attenuation, $\ln[S(\mathbf{b})/S(0)]$, and each diagonal component of $\mathbf{D}$ (*13*). Figures 3a and 3b give examples of imaging pulse sequences with trapezoidal or sinusoidal diffusion gradients. The gradient intensities are as follow: $G_1 = (G_{sl})$, a 90° slice-selection gradient; $G_2 = (G_{rdp}, G_{pe}$, or $G_{srf})$, the read-dephasing, phase-encoding, or slice-refocusing gradients, respectively; $G_3 = (G_{d_r}, G_{d_p}$, or $G_{d_s})$, the diffusion gradients in the read, phase, and slice directions, respectively; $G_4 = (G_{c_r}, G_{c_p}$, or $G_{c_s})$, the crusher gradients in the read, phase, and slice directions, respectively; $G_5 = (\frac{1}{2}G_{sl})$, a 180° slice-selection gradient; and $G_6 = (G_{ro})$, the readout gradient.

In the read direction ($b_{rr} = b_{read}$), $G_1 = 0$, $G_2 = G_{rdp}$, $G_3 = G_{d_r}$, $G_4 = G_{c_r}$, $G_5 = 0$, and $G_6 = G_{ro}$, the corresponding diagonal element of the b matrix reduces to

$$\begin{aligned} b_{rr} = \gamma^2\{ &G_{rdp}^2\tau_{22} + 2G_{d_r}G_{rdp}\tau_{23} + 2G_{c_r}G_{rdp}\tau_{24} + G_{d_r}^2\tau_{33} \\ &+ G_{c_r}^2\tau_{44} + 2G_{c_r}G_{d_r}\tau_{34} + G_{ro}^2\tau_{66} + 2G_{ro}G_{rdp}\tau_{26}\}. \end{aligned} \quad [11]$$

In the phase direction ($b_{pp} = b_{phase}$), $G_1 = 0$, $G_2 = G_{pe}$, $G_3 = G_{d_p}$, $G_4 = G_{c_p}$, $G_5 = 0$, and $G_6 = 0$, the corresponding diagonal element of the b matrix reduces to

$$\begin{aligned} b_{pp} = \gamma^2\{ &G_{pe}^2\tau_{22} + 2G_{d_p}G_{pe}\tau_{23} + 2G_{c_p}G_{pe}\tau_{24} \\ &+ G_{d_p}^2\tau_{33} + G_{c_p}^2\tau_{44} + 2G_{c_p}G_{d_p}\tau_{34}\}. \end{aligned} \quad [12a]$$

Thus, b_{pp} varies as G_{pe} is incremented. However, most b-factor calculations assume that $G_{pe} = 0$, corresponding to

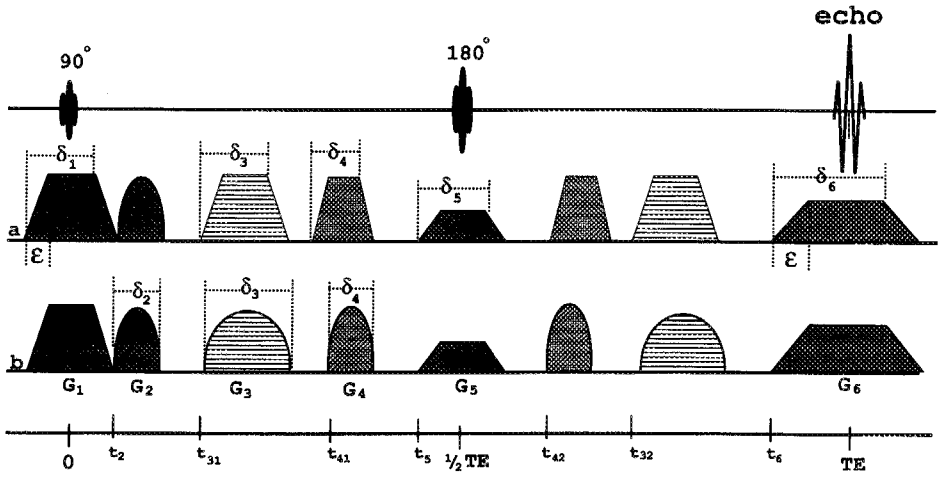

FIG. 2. The generalized imaging gradient-pulse sequences used to derive the analytical b-matrix expressions. In this figure G_{ki} (k = 1 through 6) are the gradient-pulse strengths in the ith coordinate direction (i.e., the read, phase, or slice direction). The different gradients are G_1, the 90° slice-selection gradient; G_2, a phase-encode, read-dephase, or slice-refocusing gradient; G_3, a diffusion gradient; G_4, a crusher gradient; G_5, the 180° slice-selection gradient; and G_6, the readout gradient. δ_k is the pulse duration, ϵ is the rise time of the trapezoidal ramp, and t_k is the time at which the gradient pulse turns on. In this figure, gradient pulses are shown with (a) trapezoidal or (b) sinusoidal diffusion and crusher gradients.

the center line of Fourier space in the phase-encode direction (i.e., at the top of the echo). With this condition, the expression further reduces to

$$b_{pp} = \gamma^2\{G_{d_p}^2\tau_{33} + G_{c_p}^2\tau_{44} + 2G_{c_p}G_{d_p}\tau_{34}\}. \quad [12b]$$

In the slice direction ($b_{ss} = b_{slice}$), $G_1 = G_{sl}$, $G_2 = G_{rsf}$, $G_3 = G_{d_s}$, $G_4 = G_{c_s}$, $G_5 = \frac{1}{2}G_{sl}$, and $G_6 = 0$, the corresponding diagonal element of the b matrix reduces to

$$\begin{aligned} b_{ss} = \gamma^2\{&G_{sl}^2(\tau_{11} + \tau_{15} + \tfrac{1}{4}\tau_{55}) + 2G_{sl}G_{srf}(\tau_{12} + \tfrac{1}{2}\tau_{25}) \\ &+ 2G_{sl}G_{d_s}(\tau_{13} + \tfrac{1}{2}\tau_{35}) + 2G_{sl}G_{c_s}(\tau_{14} + \tfrac{1}{2}\tau_{45}) \\ &+ G_{srf}^2\tau_{22} + 2G_{d_s}G_{srf}\tau_{23} + 2G_{c_s}G_{srf}\tau_{24} \\ &+ G_{d_s}^2\tau_{33} + G_{c_s}^2\tau_{44} + 2G_{c_s}G_{d_s}\tau_{34}\}. \end{aligned} \quad [13]$$

Off-Diagonal Elements of the b Matrix (b_{ij}, $i \neq j$)

When we consider diffusion in an anisotropic medium, we must replace the scalar diffusion coefficient with a diffusion tensor and the scalar b factor by the b matrix as in Eq. [2]. Previously, only the diagonal elements (D_{rr}, D_{pp}, and D_{ss}) and their respective b factors (b_{rr}, b_{pp}, and b_{ss}) had been considered in the context of anisotropic diffusion spectroscopy (*15, 17, 18, 20*) and imaging (*5, 20, 21*); recently, the remaining six off-diagonal elements of **D** (D_{rp}, D_{rs}, D_{ps}, D_{pr}, D_{sr}, and D_{sp}) and their respective b factors (b_{rp}, b_{rs}, b_{ps}, b_{pr}, b_{sr}, and b_{sp}) have also been considered (*13*). There should be no confusion between the off-diagonal elements of the b matrix and "cross terms" (*10*) (groups of terms that may appear within an individual b factor).

The diagonal b-matrix expressions b_{rr}, b_{pp}, and b_{ss} are identical to those derived above in Eqs. [11]–[13]. By construction, the b matrix is symmetric ($b_{ij} = b_{ji}$, $b_{rp} = b_{pr}$, $b_{ps} = b_{sp}$, and $b_{rs} = b_{rs}$) so that only three of the remaining six off-diagonal elements of the b matrix need to be determined. They are

$$\begin{aligned} b_{rp} = \gamma^2\{&G_{rdp}G_{pe}\tau_{22} + (G_{d_p}G_{rdp} + G_{d_r}G_{pe})\tau_{23} \\ &+ (G_{c_p}G_{rdp} + G_{c_r}G_{pe})\tau_{24} + G_{d_r}G_{d_p}\tau_{33} + G_{c_p}G_{c_r}\tau_{44} \\ &+ (G_{c_p}G_{d_r} + G_{d_p}G_{c_r})\tau_{34} + G_{ro}G_{pe}\tau_{26}\}, \end{aligned} \quad [14]$$

$$\begin{aligned} b_{rs} = \gamma^2\{&G_{sl}G_{rdp}(\tau_{12} + \tfrac{1}{2}\tau_{25}) + G_{sl}G_{d_r}(\tau_{13} + \tfrac{1}{2}\tau_{35}) \\ &+ G_{sl}G_{c_r}(\tau_{14} + \tfrac{1}{2}\tau_{45}) + G_{ro}G_{sl}\tau_{16} + G_{srf}G_{rdp}\tau_{22} \\ &+ (G_{d_r}G_{srf} + G_{d_s}G_{rdp})\tau_{23} + (G_{c_r}G_{srf} + G_{rdp}G_{c_s})\tau_{24} \\ &+ G_{ro}G_{srf}\tau_{26} + G_{d_s}G_{d_r}\tau_{33} + G_{c_r}G_{c_p}\tau_{44} \\ &+ (G_{c_r}G_{d_s} + G_{d_r}G_{c_s})\tau_{34}\}, \end{aligned} \quad [15]$$

and

$$\begin{aligned} b_{ps} = \gamma^2\{&G_{sl}G_{pe}(\tau_{12} + \tfrac{1}{2}\tau_{25}) + G_{sl}G_{d_p}(\tau_{13} + \tfrac{1}{2}\tau_{35}) \\ &+ 2G_{sl}G_{c_p}(\tau_{14} + \tfrac{1}{2}\tau_{45}) + G_{srf}G_{pe}\tau_{22} \\ &+ (G_{d_s}G_{pe} + G_{d_p}G_{srf})\tau_{23} + (G_{c_p}G_{srf} + G_{pe}G_{c_s})\tau_{24} \\ &+ G_{d_s}G_{d_p}\tau_{33} + G_{c_p}G_{c_s}\tau_{44} \\ &+ (G_{c_p}G_{d_s} + G_{d_p}G_{c_s})\tau_{34}\}. \end{aligned} \quad [16]$$

TABLE 1

τ Table for the Spin-Echo Sequence (Trapezoidal Diffusion Pulses)

	k					
l	1 Δ_1 = TE δ_1 = sinct + ε	2 Δ_2 = TE − t_2 δ_2 = idpt	3 $\Delta_3 = t_{32} - t_{31}$ δ_3 = difft + ε	4 $\Delta_4 = t_{42} - t_{41}$ δ_4 = crut + ε	5 $\delta_5 = \delta_1$	6 δ_6 = grot + ε
1	$\frac{3}{4}\left[\delta_1^2\left(\Delta_1 - \frac{1}{3}\delta_1\right) + \frac{1}{30}\varepsilon^2 - \frac{1}{6}\delta_1\varepsilon^2\right]$					
2	$\frac{1}{\pi}\delta_1\delta_2\left(\Delta_2 - \frac{1}{2}\delta_2\right)$	$\frac{4}{\pi^2}\delta_2^2\left(\Delta_2 - \frac{5}{8}\delta_2\right)$				
3	$\frac{1}{2}\delta_1\delta_3\Delta_3$	$\frac{2}{\pi}\delta_2\delta_3\Delta_3$	$\left[\delta_3^2\left(\Delta_3 - \frac{1}{3}\delta_3\right) + \frac{1}{30}\varepsilon^2 - \frac{1}{6}\delta_3\varepsilon^2\right]$			
4	$\frac{1}{2}\delta_1\delta_4\Delta_4$	$\frac{2}{\pi}\delta_2\delta_4\Delta_4$	$\delta_3\delta_4\Delta_4$	$\left[\delta_4^2\left(\Delta_4 - \frac{1}{3}\delta_4\right) + \frac{1}{30}\varepsilon^2 - \frac{1}{6}\delta_4\varepsilon^2\right]$		
5	$\frac{1}{8}\delta_1\left(\delta_5^2 + \frac{1}{3}\varepsilon^2\right)$	$\frac{1}{2\pi}\delta_2\left(\delta_5^2 + \frac{1}{3}\varepsilon^2\right)$	$\frac{1}{4}\delta_3\left(\delta_5^2 + \frac{1}{3}\varepsilon^2\right)$	$\frac{1}{4}\delta_4\left(\delta_5^2 + \frac{1}{3}\varepsilon^2\right)$	$\frac{1}{2}\left(\frac{1}{6}\delta_5^3 + \frac{1}{30}\varepsilon^3\right)$	
6	$-\frac{1}{16}\delta_1\left(\delta_6^2 + \frac{1}{3}\varepsilon^2\right)$	$-\frac{1}{4\pi}\delta_2\left(\delta_6^2 + \frac{1}{3}\varepsilon^2\right)$	0	0	0	$\frac{1}{4}\left(\frac{1}{6}\delta_6^3 + \frac{1}{30}\varepsilon^3\right)$

Note. Listed are the imaging parameters used to describe the pulse sequence (the functional form of the gradient pulse, e.g., its shape, duration, and magnitude) shown in Figs. 2a and 3a. The timing parameters used in the analytical expression for the trapezoidal b matrix are given in this table. The abbreviations used in these parameters are as follows: δ_k is the kth gradient-pulse duration (k-1 through 6), i.e., either the time between the initial rise of a trapezoidal pulse and the end of its plateau or the pulse duration for nontrapezoidal gradient-pulse shapes, and ε is the rise time for the trapezoidal ramp. The times at which the gradient pulses begin are given by t_i: $-t_2$ for G_1; t_2 for G_2; t_{31} for the first diffusion gradient G_3; t_{41} for the first crusher gradient G_4; t_5 for G_5; t_{32} for the second diffusion gradient G_3; t_{42} for the second crusher gradient G_4; and t_6 for G_6. The time between the kth gradient pulses in the pulse sequence Δ_k is given by $\Delta_2 = (\mathrm{TE} - t_2)$, the interval between echo time and refocusing gradients; $\Delta_3 = (t_{32} - t_{31})$, the interval between the diffusion gradients; and $\Delta_4 = (t_{42} - t_{41})$, the interval between the crusher gradients. Note that $\tau_{kl} = \tau_{lk}$.

Here, also, G_{pe} is usually set to zero (the center line of Fourier space). These equations allow us to calculate the off-diagonal elements of the b matrix for an imaging sequence, shown in Fig. 3, in which the diffusion gradients are applied in any of the three imaging directions.

EXPERIMENTAL METHODS AND RESULTS

We performed numerical integration of Eqs. [3] and [5] to determine the scalar b-factor values, using a program written in IDL (Interactive Data Language, Research System, Inc., Boulder, Colorado), as described by LeBihan *et al.* (6). We also calculated the analytical b-matrix values from Eqs. [11]–[16] using Mathematica (Wolfram Research, Inc., Champaign, Illinois) and computed both the diagonal and the off-diagonal b-matrix elements using the analytical expressions from Eqs. [11]–[16].

For the trapezoidal diffusion gradients, a comparison of the numerical and analytical diagonal b-matrix values was performed. The gradient-pulse parameters were taken from a typical imaging protocol for a 4.7 T spectroscopy/imaging system (GE Omega, Fremont, California), with phase-encode steps = 128, slice thickness = 2 mm, block size = 256, ramp time = 200 μs, and TE = 40,000 μs. The other imaging parameters are defined in Table 3; our 4.7 T magnet is capable of producing 2.0 G/mm maximum gradient strengths in any coordinate direction. By inserting the parameters into the three expressions for the diagonal components of the b matrix, Eqs. [11]–[13], with no crusher gradients, $G_{c_i} = 0.0$ G/mm, and $G_{pe} = 0.0$ G/mm, we obtain

$$b_{\mathrm{read}} = 5.96 + 68.84G_{d_r} + 280.22G_{d_r}^2, \qquad [17a]$$

$$b_{\mathrm{phase}} = 280.22G_{d_p}^2, \qquad [17b]$$

and

$$b_{\mathrm{slice}} = 0.15 + 1.314G_{d_s} + 280.22G_{d_s}^2. \qquad [17c]$$

With crusher gradients applied, G_{c_r}, G_{c_p}, and $G_{c_s} = 0.1$ G/mm, and $G_{pe} = 0.0$ G/mm,

$$b_{\mathrm{read}} = 7.58 + 80.47G_{d_r} + 280.22G_{d_r}^2, \qquad [18a]$$

$$b_{\mathrm{phase}} = 0.28 + 11.64G_{d_p} + 280.22G_{d_p}^2, \qquad [18b]$$

and

$$b_{\mathrm{slice}} = 0.50 + 12.95G_{d_s} + 280.22G_{d_s}^2. \qquad [18c]$$

With crusher gradients applied, G_{c_r}, G_{c_p}, and $G_{c_s} = 0.5$ G/mm, and $G_{pe} = 0.0$ G/mm,

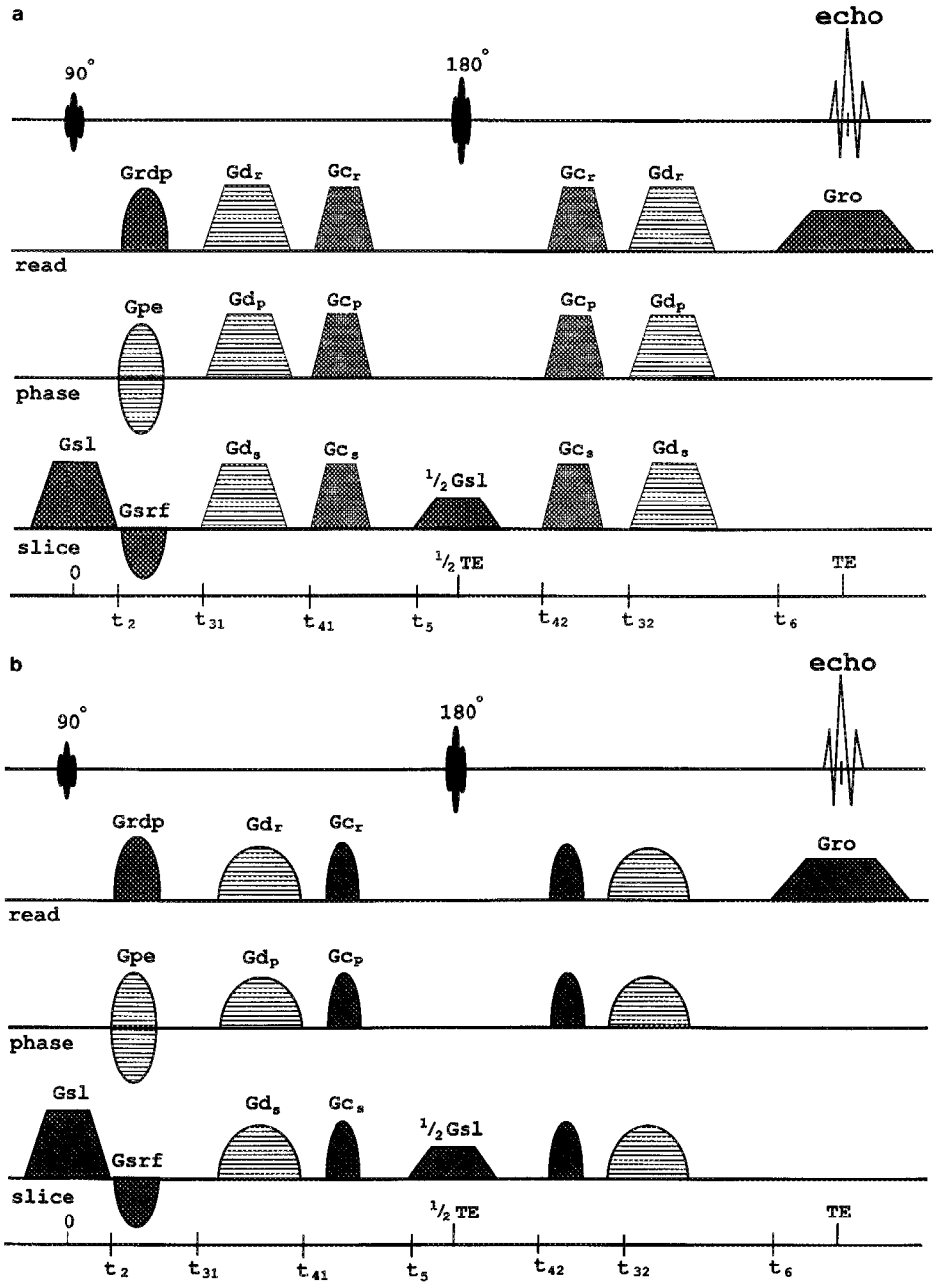

FIG. 3. The 2D FT spin-echo pulsed-gradient sequence used to acquire the diffusion-weighted images. The 90° and 180° RF pulses and the echo signal are illustrated. The time at which the gradient pulse turns on during the pulse sequence (t_k), as well as gradient pulses in the read, phase, and slice directions, is shown. Other parameters are identical with those given in the legend to Table 1. In this figure, the gradient pulses are shown with (a) trapezoidal or (b) sinusoidal diffusion and crusher gradients.

$$b_{\text{read}} = 19.66 + 127.03G_{d_r} + 280.22G_{d_r}^2, \quad [19a]$$

$$b_{\text{phase}} = 6.98 + 58.19G_{d_p} + 280.22G_{d_p}^2, \quad [19b]$$

and

$$b_{\text{slice}} = 7.47 + 59.5G_{d_s} + 280.22G_{d_s}^2. \quad [19c]$$

The diffusion gradients, G_{d_r}, G_{d_p}, and G_{d_s}, are in G/mm; the b matrix is given in s/mm^2.

The parameters in Table 3 were used to compare the analytical b-matrix values and those calculated numerically. The calculated diagonal b-matrix values agreed to within four significant digits for both trapezoidal and sinusoidal diffusion gradients in the read, phase, and slice directions.

TABLE 2
τ Table for the Spin-Echo Sequence (Sinusoidal Diffusion Pulses)

	k					
l	1 Δ_1 = TE δ_1 = sinct + ε	2 Δ_2 = TE − t_2 δ_2 = idpt	3 $\Delta_3 = t_{32} - t_{31}$ δ_3 = dift	4 $\Delta_4 = t_{42} - t_{41}$ δ_4 = crut	5 $\delta_5 = \delta_1$	6 δ_6 = grot + ε
1	$\frac{1}{4}\left[\delta_1^2\left(\Delta_1 - \frac{1}{3}\delta_1\right) + \frac{1}{30}\varepsilon^2 - \frac{1}{6}\delta_1\varepsilon^2\right]$					
2	$\frac{1}{\pi}\delta_1\delta_2\left(\Delta_2 - \frac{1}{2}\delta_2\right)$	$\frac{4}{\pi^2}\delta_2^2\left(\Delta_2 - \frac{5}{8}\delta_2\right)$				
3	$\frac{1}{\pi}\delta_1\delta_3\Delta_3$	$\frac{4}{\pi^2}\delta_2\delta_3\Delta_3$	$\frac{4}{\pi^2}\delta_3^2\left(\Delta_3 - \frac{1}{4}\delta_3\right)$			
4	$\frac{1}{\pi}\delta_1\delta_4\Delta_4$	$\frac{4}{\pi^2}\delta_2\delta_4\Delta_4$	$\frac{4}{\pi^2}\delta_3\delta_4\Delta_4$	$\frac{4}{\pi^2}\delta_4^2\left(\Delta_4 - \frac{1}{4}\delta_4\right)$		
5	$\frac{1}{8}\delta_1\left(\delta_5^2 + \frac{1}{3}\varepsilon^2\right)$	$\frac{1}{2\pi}\delta_2\left(\delta_5^2 + \frac{1}{3}\varepsilon^2\right)$	$\frac{1}{2\pi}\delta_3\left(\delta_5^2 + \frac{1}{3}\varepsilon^2\right)$	$\frac{1}{2\pi}\delta_4\left(\delta_5^2 + \frac{1}{3}\varepsilon^2\right)$	$\frac{1}{2}\left(\frac{1}{6}\delta_5^3 + \frac{1}{30}\varepsilon^3\right)$	
6	$-\frac{1}{16}\delta_1\left(\delta_6^2 + \frac{1}{3}\varepsilon^2\right)$	$-\frac{1}{4\pi}\delta_2\left(\delta_6^2 + \frac{1}{3}\varepsilon^2\right)$	0	0	0	$\frac{1}{4}\left(\frac{1}{6}\delta_6^3 + \frac{1}{30}\varepsilon^3\right)$

Note. Listed are the imaging parameters used to describe the pulse sequence (the functional form of the gradient pulse, e.g., its shape, duration, and magnitude) shown in Figs. 2b and 3b. The timing parameters used in the analytical expression for the sinusoidal b matrix are defined in this table. The abbreviations for these parameters are the same as those described in the legend to Table 1. Note that $\tau_{kl} = \tau_{lk}$.

To validate the diagonal b-matrix values, we obtained coronal images (64 × 64 pixels) of two isotropic materials, water and polyacrylamide gel phantoms, with the diffusion gradient varying from 0 to 1.5 G/mm, in each of the three coordinate directions (read, phase, and slice). We measured the temperature of the phantom using Luxtron fiberoptic probes, and the images were acquired when the system was at a stable temperature. For the water phantom, the slice thickness was 4 mm, the ramp time was 1.0 ms, the field of view was 40 mm, and TE was 120 ms. For the polyacrylamide gel phantom, the slice thickness was 10 mm, the ramp time was 0.5 ms, the field of view was 64 mm, and TE was 100 ms. Other imaging parameters for these experiments are given in Table 3.

The cross terms in Eqs. [17]–[19], consisting of those terms that do not depend on the square of the diffusion gradient ($G_{d_i}G_{d_j}$), are significant especially for small diffusion-gradient values. In order to assess the error we make in ignoring them, we must compare the estimates of the diffusivity with and without these cross terms. First, we use Eq. [9], which assumes no contribution from the imaging gradients, to estimate the diffusivity using Eq. [1]. We then use Eqs. [11]–[13], which take into account the other imaging gradients, and repeat the estimation of the diffusivity. A linear regression program, adapted from Bevington (*22*), was used to calculate the diffusion coefficient, the standard deviation, and the reduced weighted χ^2 statistics. Figures 4 and 5 show plots of Eq. [1] in the three orthogonal directions. The diagonal b-matrix values used to fit the data were calculated from Eq. [9] and Eq. [11], [12], or [13]. In using Eqs. [11]–[13], which take into account the cross terms, we see that both the linearity of the data points and the equality of the estimated diffusion coefficients in the three directions support the conclusion that the b-matrix values were calculated correctly.

For the water phantom (Fig. 4), the diffusion coefficients at 16.0°C estimated using Eqs. [11], [12], and [13], respectively, were $D_{\text{read}} = (1.74 \pm 0.06) \times 10^{-3}$ mm^2/s, $\chi^2 = 0.0009$, $D_{\text{phase}} = (1.71 \pm 0.06) \times 10^{-3}$ mm^2/s, $\chi^2 = 0.0009$, and $D_{\text{slice}} = (1.74 \pm 0.06) \times 10^{-3}$ mm^2/s, $\chi^2 = 0.0018$, which are the same to within experimental error. This conclusion is further supported by comparing these estimated diffusivities with the spectroscopically obtained estimated diffusion coefficient. In this experiment, we estimated that $D = (1.74 \pm 0.03) \times 10^{-3}$ mm^2/s, $\chi^2 = 0.04$, whereas, using Eq. [9], which ignores cross terms, produced data points that were noncollinear, and resulted in an incorrect estimated diffusivity: $D_{\text{read}} = (1.50 \pm 0.06) \times 10^{-3}$ mm^2/s, $\chi^2 = 0.018$, $D_{\text{phase}} = (1.48 \pm 0.06) \times 10^{-3}$ mm^2/s, $\chi^2 = 0.02$, and $D_{\text{slice}} = (1.64 \pm 0.06) \times 10^{-3}$ mm^2/s, $\chi^2 = 0.11$.

For the polyacrylamide gel phantom (Fig. 5), the diffusion coefficients at 16.0°C estimated using Eqs. [11], [12], and [13], respectively, were $D_{\text{read}} = (1.47 \pm 0.05) \times 10^{-3}$ mm^2/s, $\chi^2 = 0.003$, $D_{\text{phase}} = (1.45 \pm 0.05) \times 10^{-3}$ mm^2/s, $\chi^2 = 0.0005$, and $D_{\text{slice}} = (1.43 \pm 0.04) \times 10^{-3}$ mm^2/s, $\chi^2 = 0.0008$, which are the same to within experimental error. This conclusion is further supported by comparing these estimated diffusivities with the spectro-

TABLE 3
Parameters Used to Calculate the *b*-Matrix Values for the Three Experiments

	Numerical and analytical parameters		
i	δ_i (μs)	t_i (μs)	G_i (G/mm)
1	2200.0	−1200.0	G_{sl} +0.352 G_{rdp} +0.381
2	2000.0	1200.0	G_{pe} +0.000 G_{srf} −0.304
3	4200.0[a]		G_{d_r} 0 to +1.400
(31)		6000.0[b]	G_{d_p} 0 to +1.400 G_{d_s} 0 to +1.400
4	2200.0[a]		G_{c_r} 0 or +0.500
(41)		14400.0[b]	G_{c_p} 0 or +0.500 G_{c_s} 0 or +0.500
5	2200.0	18800.0	
(42)		23200.0	
(32)		29600.0[b]	
6	6614.5	36592.75	G_{ro} +0.147

	Water imaging parameters			Polyacrylamide gel imaging parameters		
i	δ_i (μs)	t_i (μs)	G_i (G/mm)	δ_i (μs)	t_i (μs)	G_i (G/mm)
1	2950.0	−1975.0	G_{sl} −0.301 G_{rdp} −0.241	4375.0	−2437.5	G_{sl} −0.061 G_{rdp} −0.122
2	2000.0	1975.0	G_{pe} +0.000 G_{srf} +0.349	2000.0	2437.5	G_{pe} +0.000 G_{srf} +0.104
3	5000.0		G_{d_r} 0 to −1.500	4500.0		G_{d_r} 0 to −1.400
(31)		24025.0	G_{d_p} 0 to +1.500 G_{d_s} 0 to −1.500		9562.5	G_{d_p} 0 to +1.400 G_{d_s} 0 to −1.400
4	3000.0		G_{c_r} 0 or −0.300	2500.0		G_{c_r} −0.500
(41)		50025.0	G_{c_p} 0 or +0.300 G_{c_s} 0 or −0.300		24562.5	G_{c_p} +0.500 G_{c_s} −0.500
5	2950.0	58025.0		4375.0	47562.5	
(42)		65975.0			72437.5	
(32)		89975.0			85437.5	
6	2614.5	118192.75	G_{ro} −0.235	2114.5	98692.75	G_{ro} −0.147

Note. The kth gradient-pulse strengths (G_k), the gradient-pulse durations (δ_k), and the time during which the gradient pulses are turned on during the pulse sequences (t_k) are defined in the caption to Table 1.

[a] For sinusoidal diffusion and crusher gradients, these values are $\delta_3 = 4000.0$ and $\delta_4 = 2000.0$ μs.

[b] For sinusoidal diffusion and crusher gradients, these values are $t_{31} = 6800.0$, $t_{41} = 14800.0$, and $t_{32} = 29200.0$ μs.

scopically obtained estimated diffusion coefficient. In this experiment, we estimated that $D = (1.43 \pm 0.06) \times 10^{-3}$ mm^2/s, $\chi^2 = 0.001$. In contrast, use of Eq. [9], which ignores cross terms, produced data points that were non-collinear, and resulted in an incorrect estimated diffusivity: $D_{read} = 6.76 \times 10^{-3}$ mm^2/s, $\chi^2 = 6.57$, $D_{phase} = 6.34 \times 10^{-3}$ mm^2/s, $\chi^2 = 5.70$, and $D_{slice} = 6.12 \times 10^{-3}$ mm^2/s, $\chi^2 = 8.11$.

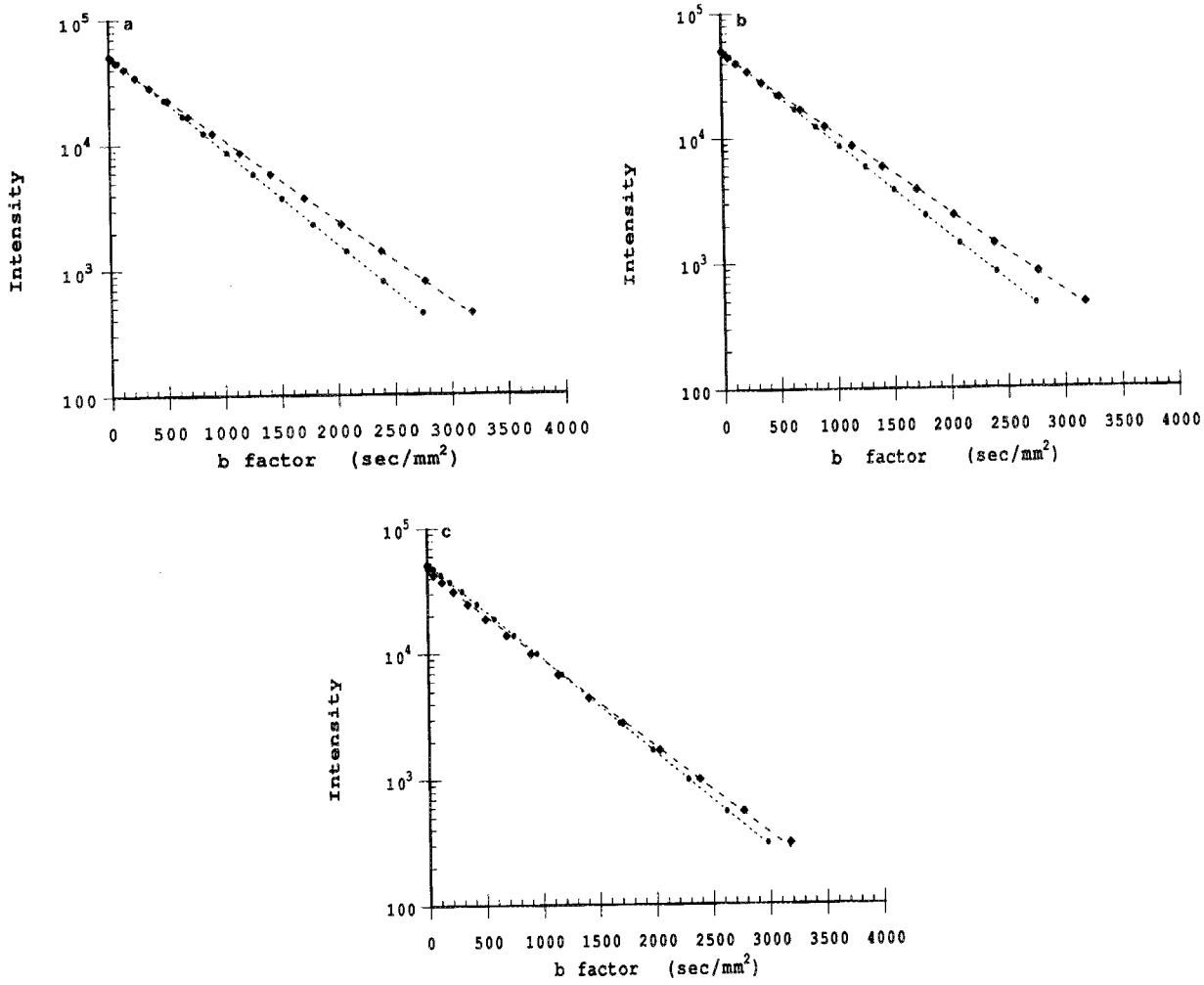

FIG. 4. The signal intensity versus the diagonal b matrix for the three directions (read, phase, and slice) for the water phantom: (a) x direction (phase), (b) y direction (slice), and (c) z direction (read). Using Eqs. [11], [12], and [13], we see that both the goodness of fit and the agreement with the diffusivities estimated from imaging and spectroscopic measurements indicate that the b-matrix values were calculated correctly (●). To demonstrate the effect of cross terms on the estimation of the diffusivity, we also calculated the scalar b factors using Eq. [9], intentionally omitting the cross terms (♦). Both the poor fit and the significant disagreement with the diffusivity estimated from spectroscopic measurements demonstrate that calculating the b factors without the cross terms leads to significant errors in the estimation of diffusivities.

The parameter values from Table 3 were used to calculate a b matrix when no diffusion gradients are present:

$$\mathbf{b}(0, 0, 0) = \begin{bmatrix} 19.66 & 10.34 & 10.62 \\ 10.34 & 6.98 & 7.15 \\ 10.62 & 7.15 & 7.41 \end{bmatrix}.$$

Similarly, when only the read diffusion gradients (G_{dr}) are equal to 1.0 G/mm, the b matrix is

$$\mathbf{b}(1, 0, 0) = \begin{bmatrix} 426.91 & 10.34 & 40.37 \\ 10.34 & 6.98 & 7.15 \\ 10.62 & 7.15 & 7.41 \end{bmatrix}.$$

When only the read and slice (G_{dr} and G_{ds}) diffusion gradients are equal to 1.0 G/mm, the b matrix is

$$\mathbf{b}(1, 0, 1) = \begin{bmatrix} 426.91 & 39.43 & 384.11 \\ 39.43 & 6.98 & 36.24 \\ 384.11 & 36.24 & 347.19 \end{bmatrix}.$$

Finally, when all three diffusion gradients, read, phase, and slice, are equal to 1.0 G/mm, the b matrix is

$$\mathbf{b}(1, 1, 1) = \begin{bmatrix} 426.91 & 383.17 & 384.11 \\ 383.17 & 345.39 & 346.22 \\ 384.11 & 346.22 & 347.19 \end{bmatrix}.$$

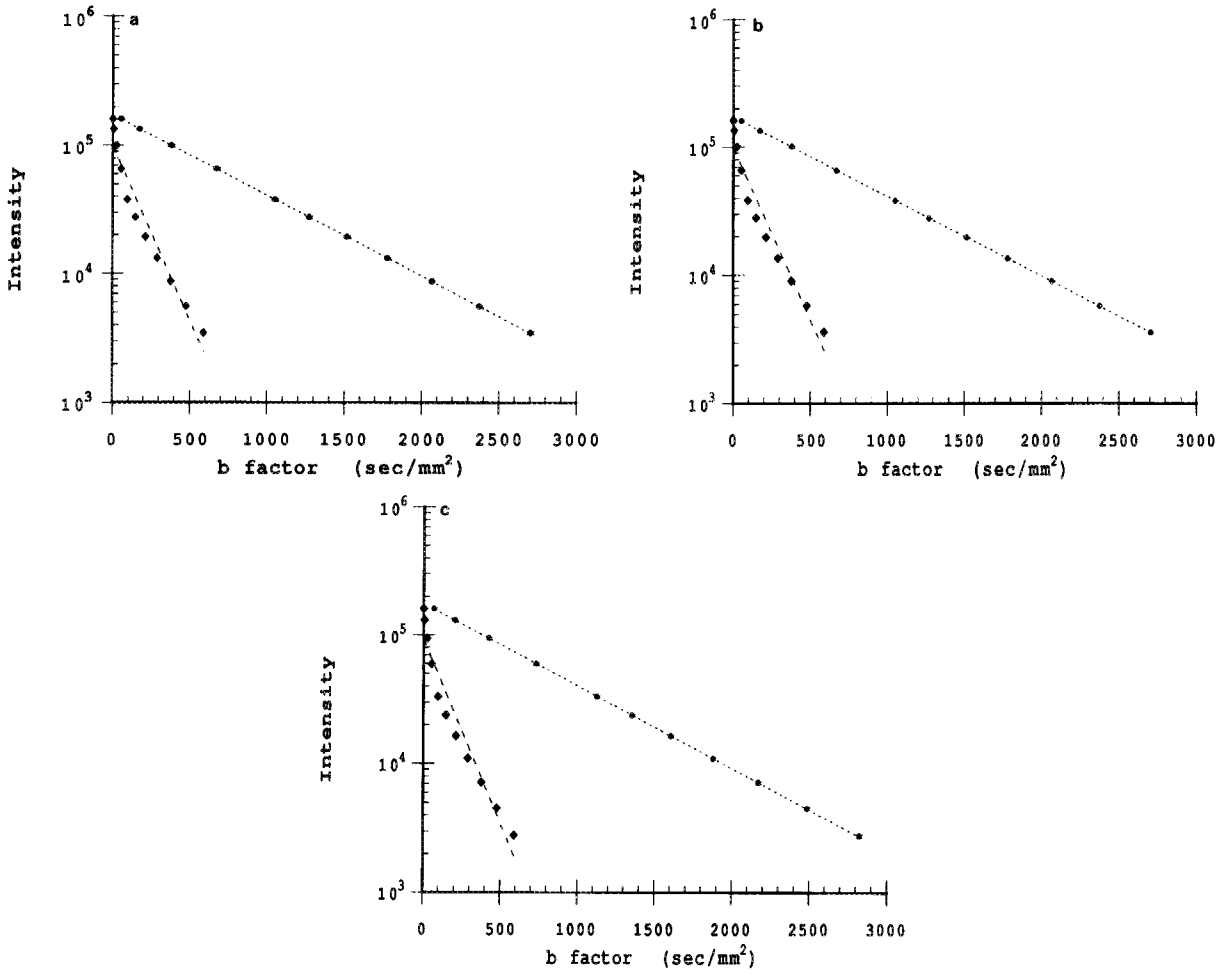

FIG. 5. The signal intensity versus the diagonal b matrix for the three directions (read, phase, and slice) for the polyacrylamide gel phantom: (a) x direction (phase), (b) y direction (slice), and (c) z direction (read). Using Eqs. [11], [12], and [13], we see that both the goodness of fit and the agreement with the diffusivities estimated from imaging and spectroscopic measurements indicate that the b-matrix values were calculated correctly (indicated by ●). To demonstrate the effect of cross terms on the estimation of the diffusivity, we also calculated the scalar b factors using Eq. [9], intentionally omitting the cross terms (♦). Both the poor fit and the significant disagreement with the diffusivity estimated from spectroscopic measurements demonstrate that calculating the b factors without the cross terms leads to significant errors in the estimation of diffusivities.

These b matrices illustrate the significance of the cross terms, and the magnitude of the off-diagonal compared to the diagonal elements.

DISCUSSION AND CONCLUDING REMARKS

The proposed analytical expressions of the b matrix permit accurate and efficient determination of the diagonal and off-diagonal elements of the effective diffusion tensor in NMR diffusion spectroscopy and imaging. The goodness of fit to Eq. [1] of the imaging data shows that the calculated b matrix used in Eqs. [11]–[13] explains the diffusion data well. The b-matrix values are calculated in the pulse sequence and are automatically inserted into the image file headers. The imaging data from the water and polyacrylamide gel showed that the diffusion coefficient in each of the three coordinate directions are similar, within allowable experimental error.

Our work confirms that ignoring cross terms can introduce significant errors into the estimate of the diffusion coefficient. Using analytical expressions or numerically evaluated b-matrix values eliminates this source of error.

In order to achieve the largest value of the b matrix for a given pulse sequence, one should choose the orientation of the diffusion and crusher gradients to be the same orientation as those the other imaging gradients along that coordinate direction. That is, if the readout gradients are positive or negative, the crusher and diffusion gradients should be positive or negative, respectively. Likewise, if the 90° and 180° slice-selection and crusher gradients are positive or negative, the diffusion gradient in the slice direction should be positive

or negative, respectively. Otherwise, the interactions between the imaging, crusher, and diffusion gradients would reduce the magnitude of the b factor.

Whether the diffusion gradients are zero or not, the components of the b matrix are significant and off-diagonal components can be as large as the diagonal components. The b-matrix values given at the end of Experimental Methods and Results show that, when the diffusion gradient is zero, the b matrix may still have small nonzero values. When a diffusion gradient is applied in only one direction (such as the read), all diagonal and off-diagonal b-matrix elements become significantly different from zero. For the case where diffusion gradients in two directions are nonzero (read and slice), these diagonal b-matrix elements and all of the off-diagonal elements are significantly different from the zero b-matrix values. When all diffusion gradients are nonzero, all of the b-matrix elements are significantly different from the zero b-matrix values. Using only a scalar b factor, which ignores these off-diagonal elements, results in an incorrect estimate of the diffusion coefficient. These off-diagonal components are needed to estimate the components of the effective diffusion tensor, and to perform diffusion tensor imaging (DTI) as described by Basser *et al.* (*13, 23*).

ACKNOWLEDGMENTS

This work was performed at the NIH *in Vivo* NMR Center. We thank Alan Olson and Scott Chesnick for their technical support. We thank Barry Bowman and Brad Roth for editing this manuscript.

REFERENCES

1. D. LeBihan, R. Turner, P. Douek, and N. Patronas. *Am. J. Radiol.* **159,** 591 (1992).
2. C. T. W. Moonnen, M. von Kienlin, P. C. M. van Zijl, J. Cohen, J. Gillen, P. Daly, and G. Wolf. *NMR Biomed.* **2,** 201 (1989).
3. C. T. W. Moonnen, P. C. M. van Zijl, d. LeBihan, and D. DesPres, *Magn. Reson. Med.* **13**(3), 467 (1990).
4. S. Posse, C. A. Cuenod, and D. LeBihan, Abstracts of the Society of Magnetic Resonance in Medicine, 11th Annual Meeting, Berlin, Germany, p. 2141, 1992.
5. D. G. Taylor and M. C. Bushell, *Phys. Med. Biol.* **30,** 345 (1985).
6. D. LeBihan, E. Breton, D. Lallemond, P. Grenier, E. Cabanis, and M. Laval-Jeantet, *Radiology* **161,** 401 (1986).
7. K. D. Merboldt, W. Hanicke, and J. Frahm, *J. Magn. Reson.* **64,** 479 (1985).
8. R. Turner, D. LeBihan, J. Maier, R. Vavrek, L. K. Hedges, and J. Pekar, *Radiology* **177,** 407 (1990).
9. D. LeBihan, C. A. Cuenod, and S. Posse, Abstracts of the Society of Magnetic Resonance in Medicine, 11th Annual Meeting, Berlin, Germany, p. 1218, 1992.
10. M. Neeman, J. P. Freyer, and L. O. Sillerud, *J. Magn. Reson.* **90,** 303 (1990).
11. G. G. Cleveland, D. G. Chang, C. F. Hazlewood, and H. E. Rorschach, *Biophys. J.* **16,** 1043 (1976).
12. M. E. Moseley, Y. Cohen, J. Kucharczyk, J. Mintorovitch, H. S. Asgari, M. F. Wendland, J. Tsuruda, and D. Norman, *Radiology* **176,** 439 (1990).
13. P. J. Basser, J. Mattiello, and D. LeBihan, *J. Magn. Reson.*, in press (1993).
14. H. C. Torrey, *Phys. Rev.* **104,** 563 (1956).
15. E. O. Stejskal, *J. Chem. Phys.* **43,** 3597 (1965).
16. E. L. Hahn, *Phys. Rev.* **80,** 580 (1950).
17. H. Y. Carr and E. M. Purcell, *Med. Phys.* **94,** 930 (1954).
18. J. H. Simpson and H. Y. Carr, *Phys. Rev.* **111,** 1201 (1958).
19. E. O. Stejskal and J. E. Tanner, *J. Chem. Phys.* **42,** 288 (1965).
20. W. S. Price and P. W. Kuchel, *J. Magn. Reson.* **94,** 133 (1991).
21. D. LeBihan, *Magn. Reson. Quart.* **7,** 1 (1991).
22. P. R. Bevington, "Data Reduction and Error Analysis for the Physical Sciences," p. 172, McGraw–Hill, New York, 1969.
23. P. J. Basser, J. Mattiello, and D. LeBihan, *Biophys. J.*, in press (1993).